PROTEINS: Structure, Function, and Genetics 4:283–293 (1988)

Crystallographic Studies of Inhibitor Binding Sites in Human Carbonic Anhydrase II: A Pentacoordinated Binding of the SCN^- Ion to the Zinc at High pH

A. Elisabeth Eriksson, Per M. Kylsten, T. Alwyn Jones, and Anders Liljas
Department of Molecular Biology, Biomedical Center, S-751 24 Uppsala, Sweden

ABSTRACT **The binding of four inhibitors—mercuric ion, 3-acetoxymercuri-4-aminobenzenesulfonamide (AMS), acetazolamide (Diamox), and thiocyanate ion—to human carbonic anhydrase II (HCA II) has been studied with X-ray crystallography.**

The binding of mercury to HCA II at pH 7.0 has been investigated at 3.1 Å resolution. Mercuric ions are observed at both nitrogens in the His-64 ring. One of these sites is pointing toward the zinc ion. The only other binding site for mercury is at Cys-206.

The binding of the two sulfonamide inhibitors AMS and Diamox, has been reinvestigated at 2.0 and 3.0 Å, respectively. Only the nitrogen of the sulfonamide group binds to the zinc ion replacing the hydroxyl ion. The sulfonamide oxygen closest to the zinc ion is 3.1 Å away. Thus the tetrahedral geometry of the zinc is retained, refuting earlier models of a pentacoordinated zinc.

The structure of the thiocyanate complex has been investigated at pH 8.5 and the structure has been refined at 1.9 Å resolution using the least-squares refinement program PROLSQ. The crystallographic *R* factor is 17.6%. The zinc ion is pentacoordinated with the anion as well as a water molecule bound in addition to the three histidine residues. The nitrogen atom of the SCN^- ion is 1.9 Å from the zinc ion but shifted 1.3 Å with respect to the hydroxyl ion in the native structure and at van der Waals' distance from the Oγl atom of Thr-199. This is due to the inability of the Oγl atom of Thr-199 to serve as a hydrogen bond donor, thus repelling the nonprotonated nitrogen. The SCN^- molecule reaches into the deep end of the active site cavity where the sulfur atom has displaced the so-called "deep" water molecule of the native enzyme. The zinc-bound water molecule is 2.2 Å from the zinc ion and 2.4 Å from the SCN^- nitrogen. In addition, this water is hydrogen bonded to the Oγl atom of Thr-199 and to another water molecule.

We have observed that solvent and inhibitor molecules have three possible binding sites on the zinc ion and their significance for the catalysis and inhibition of HCA II will be discussed. All available crystallographic data are consistent with a proposed catalytic mechanism in which both the OH moiety and one oxygen of the substrate HCO_3^- ion are ligated to the zinc ion.

Key words: crystallography, structure, refinement, sulfonamide, thiocyanate, mercury

INTRODUCTION

The catalytic mechanism for carbonic anhydrase enzymes (CA) includes a direct nucleophilic attack of the zinc-bound hydroxyl ion on a substrate CO_2 molecule. In some models a pentacoordinated zinc intermediate has been suggested[1] but has not been generally accepted:

To delineate the mechanism of CA one useful tool has been to study the effects of different inhibitors. The major inhibitors are sulfonamides and monovalent anions but other types of inhibitors exist such as the divalent metal ions Cu^{2+} and Hg^{2+}. We have studied the binding sites of inhibitors from these three classes by crystallographic techniques.

That bicarbonate ion has two of its oxygens bound to the zinc ion has partly been supported by the crystallographic interpretations that sulfonamide inhibitors bind in a pentacoordinated fashion to the zinc ion both in HCA I and HCA II.[2] However, these results were based on phases from the unrefined structure. Therefore we have now reinvestigated the binding of the two inhibitors, 3-acetoxymercuri-4-aminobenzenesulfonamide (AMS) and acetazolamide (Diamox) with phase angles calculated from the refined structure of HCA II.[3]

The thiocyanate ion has higher affinity for the acidic ($Zn–H_2O$) form of CA than for the alkaline ($Zn–OH^-$) form.[4–6] The ion can principally bind to the zinc either by displacing the zinc ligand or by increasing the coordination number. UV-visible absorption spectra of SCN^--inhibited Co(II)-substituted enzyme[7,8]

Received September 6, 1988; accepted October 28, 1988.

Address reprint requests to A. Elisabeth Eriksson, Institute of Molecular Biology, University of Oregon, Eugene, OR 97403-1229.

Per M. Kylsten's present address is Department of Microbiology, University of Stockholm, S-106 91 Stockholm, Sweden.

Anders Liljas' present address is: Department of Molecular Biophysics, Chemical Center, University of Lund, Box 124, S-221 00 Lund, Sweden.

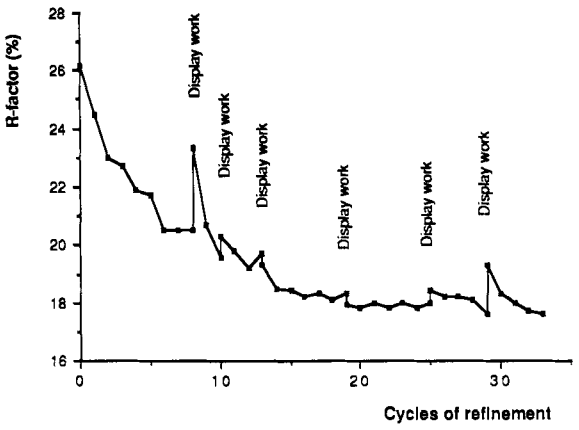

Fig. 1. Progress of the refinement of SCN^--inhibited HCA II. The crystallographic R factor ($R = \Sigma||F_{obs}| - |F_{calc}||/\Sigma|F_{obs}|$) is plotted as a function of cycle number. The resolution range of data was 7.0–1.9 Å.

have been interpreted as indicating a tetrahedral geometry around the metal at low pH and a pentacoordinated metal at high pH which would mean that both one water molecule and one SCN^- ion are bound to the zinc. We have analyzed the binding of SCN^- ion to HCA II at high pH in order to clarify the coordination geometry of the zinc.

The divalent metal ion Cu^{2+} is a weak inhibitor of CA I but a strong inhibitor of CA II.[9] Isotope exchange experiments by Tu et al.[10] have shown that Cu^{2+} does not affect the rate of either substrate binding or subsequent product release. The same effects were also observed for Hg^{2+} ions. These results indicate that the metals bind to some site other than the zinc ion and it was suggested that they bind to His-64.[10] Since this is the first report of an inhibitor binding someplace other than the zinc ion, we decided to investigate this further with X-ray crystallography.

MATERIALS AND METHODS

Hg^{2+}

HCA II is crystallized in 2.3 M ammonium sulfate and 0.05 M Tris–HCl at pH 8.5,[11] but since optimal inhibition occurs at pH 7.0[10] and because Hg^{2+} binds strongly to ammonia, Hg^{2+} ions could not be added directly to the crystallization medium. To our surprise, a direct transfer of crystals from ammonium sulfate to polyethylene glycol (PEG) 6000 was possible if performed in three steps each over a period of 1 day. First the precipitating agent was changed by transferring the crystals to 20% PEG 6000 in 0.05 M Tris–HCl, pH 8.5. The crystals were then transferred to 20% PEG 6000 in 0.05 M 2-(*N*-morpholino) ethanesulfonic acid (MES), pH 7.0. Finally they were soaked in 20% PEG 6000 in 0.05 M MES pH 7.0 with 0.1 mM $HgCl_2$. Diffraction data to 3.1 Å resolution (5332 measurements) were collected on a STOE diffractometer (Darmstadt, West Germany).[12] All data handling was performed with PROTEIN[13] unless otherwise stated. The crystals have space group $P2_1$ with cell dimensions $a = 42.8$ Å, $b = 42.1$ Å, $c = 72.7$ Å, and $\beta = 104.9°$. The native enzyme crystals dimensions are $a = 42.7$ Å, $b = 41.7$ Å, $c = 73.0$ Å, and $\beta = 104.6°$.[14] Of reflections with bad agreements 34 were rejected leaving 99% of the total data to 3.1 Å (4636 unique reflections). The R_{merge}* for the data set was 8.3%. The relative occupancies of the Hg^{2+} binding sites were approximated using Rossmann's heavy atom refinement program,[15] and with phase angles from the heavy atom positions of the AMS, methylmercurithioglycolic acid, and $Au(CN)_2^-$ derivatives.[14]

Calculated structure factor amplitudes from the highly refined model of HCA II[3] were used in electron density map calculations with $|F_{obs}(\text{complex})| - |F_{calc}(\text{native})|$ or $2|F_{obs}(\text{complex})| - |F_{calc}(\text{native}|$ as amplitudes and the calculated model phases. The active site water molecules identified in the native model were deleted and not used in the structure factor calculations. All calculations were done on a VAX 11/750 computer. The resulting electron density maps were inspected on an interactive graphics system (Vector General 3400 and Evans & Sutherland PS 300, PS 330) using the program system FRODO.[16,17] The crystallographic R factor ($\Sigma||F_{obs}| - |F_{calc}||/\Sigma|F_{obs}|$) for the Hg^{2+} complex including the three mercury ions is 23.1% at 3.1 Å resolution.

AMS and Diamox

Crystallization and data collection from AMS-[14] and Diamox-inhibited[18] HCA II have been described previously. The final concentration of inhibitor in the crystallization solution was 1 mM in both cases. Diffraction data were collected for AMS to 2.0 Å on precession cameras and for Diamox to 3.0 Å on a General Electric diffractometer.

The stereochemistry of the AMS-HCA II complex was improved by restrained least-squares refinement against the X-ray data using PROLSQ,[19] refining both position and individual temperature factors with data from 7.0 to 2.0 Å resolution (15,585 reflections). The model for the refinement was the native enzyme with three mercury ions added but no active site water molecules were included. One of these mercury ions is part of the AMS molecule but the rest of the AMS molecule was not included in the refinement. Five cycles of PROLSQ reduced the crystallographic

$$*R_{merge} = \sum_r^N \left(\sum_i^{n(r)} |I(i,r) - \langle I(r)\rangle| \right) / \sum_r^N (n(r) \times \langle I(r)\rangle) \times 100.0$$

where N is the number of unique reflections, $n(r)$ is the number of multiple measurements for the rth reflection with the mean value $\langle I(r)\rangle$ and $I(i,r)$ is the ith individual measurements of the rth reflection.

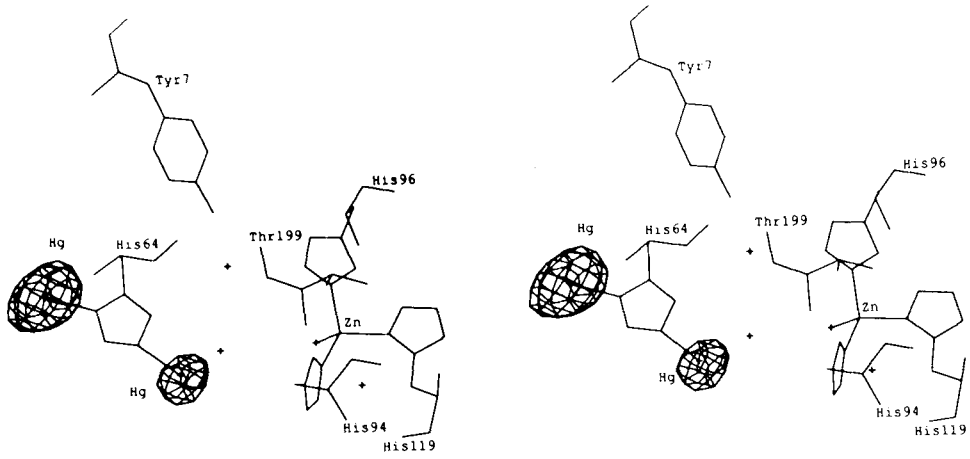

Fig. 2. Stereo view of the $|F_{obs}(complex)| - |F_{calc}(native)|$ electron density for Hg^{2+} bound to HCA II at 3.1 Å resolution. Contours are drawn at height $+5\sigma$ where σ is the rms density throughout the unit cell.

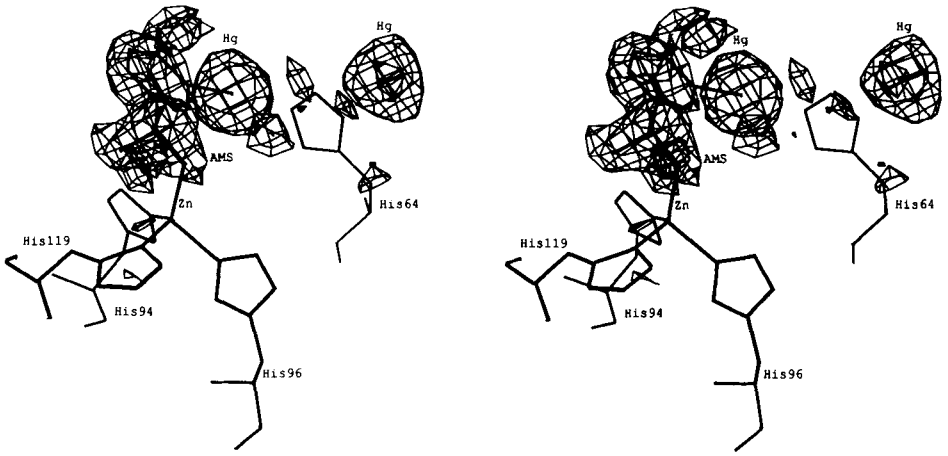

Fig. 3. Stereo view of the $|F_{obs}| - |F_{calc}|$ electron density for the active site of the AMS–HCA II complex at 2.0 Å resolution. Contours are drawn at $+2\sigma$. The AMS molecule as well as the two additional mercury ions were not included in the phase calculation. Note the resolution of the atoms of the sulfonamide group. The bad density over half the benzene ring is due to ripple effects from the more electron-dense mercury ion.

R factor from 27.0 to 19.2%. The root mean square (rms) departures from the restraints to ideal geometry were 0.028, 0.041, and 0.046 Å for bond, angle, and fixed dihedral angle distance, 0.014 Å for out of plane restrains, and 0.153 $Å^3$ for chiral volumes.[19] The deviation from the isotropic thermal factor restraints were 0.850 $Å^2$ for main chain bonds, 1.365 $Å^2$ for main chain angles, 1.001 $Å^2$ for side chain bonds, and 1.636 $Å^2$ for the side chain angles. The rms parameter shifts in the final cycle were 0.040 Å for coordinates and 0.18 $Å^2$ for temperature factors. $2|F_{obs}| - |F_{calc}|$ and $|F_{obs}| - |F_{calc}|$ electron density maps using model phases were calculated and inspected with computer graphics.

Electron density maps for the Diamox complex were calculated in the same manner as described for the Hg^{2+} complex. The crystallographic R factor for the final Diamox model is 22.3% at 3.0 Å resolution.

SCN^-

High-quality crystals of HCA II can be grown in complex only with mercury compounds such as *p*-chloromercuribenzenesulfonic acid (PCMBS). Therefore to obtain the native enzyme, crystals were soaked for 2–3 days with 0.01 M cysteine in the crystallization medium.[11] The crystals were subsequently soaked overnight with 1 mM NaSCN in the crystallization medium. X-ray diffraction data were collected at +4° C on Enraf-Nonius Arndt-Wonacott oscillation cameras (Delft, The Netherlands) using Ni-filtered

CuK_α radiation from GX-20 and GX-6 rotating anodes (Elliott Bros Ltd., England) and Reflex 25 (CEA AB, Sweden) X-ray-sensitive films. A data set of 90° around the a^* axis was recorded (23,834 measurements). The cell dimensions of the crystals did not deviate significantly from those of the native enzyme. 1019 reflections with bad agreements were rejected during data processing[20,21] leaving 67% of the total data to 1.9 Å (14,410 unique reflections). The R_{merge} for the data set was 6.7%.

A highly refined model of native HCA II with the solvent atoms in the active site removed was used as the starting model for PROLSQ refinement. A total number of 33 cycles of PROLSQ were done with six interruptions where new $2|F_{obs}| - |F_{calc}|$ or $|F_{obs}| - |F_{calc}|$ Fourier maps using model phases were calculated and inspected with computer graphics. The variation of the crystallographic R factor throughout the refinement is given in Figure 1. The SCN^- ion was included after the first nine cycles of PROLSQ. Of the 2216 atoms refined, 172 were solvent molecules associated with the enzyme. The crystallographic R factor is 17.6% for the final model including data from 7.0 to 1.9 Å resolution. The rms departures from the restraints to ideal geometry in the final refinement cycle were 0.024, 0.042, and 0.041 Å for bond, angle, and fixed dihedral angle distance, 0.012 Å for out of plane restraints, and 0.151 $Å^3$ for chiral volumes.[19] The deviation from the isotropic thermal factor restraints were 0.686 $Å^2$ for main chain bonds, 1.136 $Å^2$ for main chain angles, 0.878 $Å^2$ for side chain bonds, and 1.430 $Å^2$ for the side chain angles. The rms parameter shifts in the final cycle were 0.013 Å for coordinates and 0.11 $Å^2$ for temperature factors.

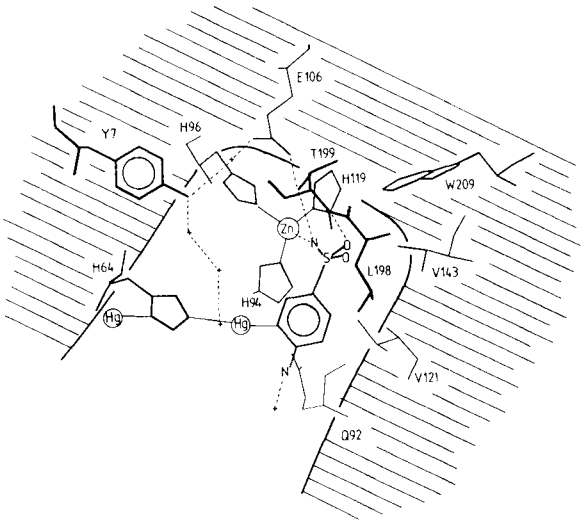

Fig. 4. Schematic drawing of the binding of the AMS inhibitor to HCA II. The molecule makes van der Waals' contacts with Val-121, Val-143, Leu-198, and Gln-92 in the hydrophobic side of the active site cavity.

RESULTS

Hg^{2+}

In the electron density map of the mercury-inhibited crystals of HCA II, Hg^{2+} ions were found to bind at three different sites. One site is situated, as expected, at the SH group of Cys-206. The two other sites are at both nitrogens of the His-64 side chain (see Fig. 2). The positions of the mercury ions are consistent with a fixed orientation of the histidine imidazole ring where the Nϵ2 atom points toward the zinc ion. The bond distance between Hg^{2+} ion and its respective nitrogen atom is about 2.2 Å. The mercury ions have no other ligands to the protein. No additional electron density peak is observed in the map

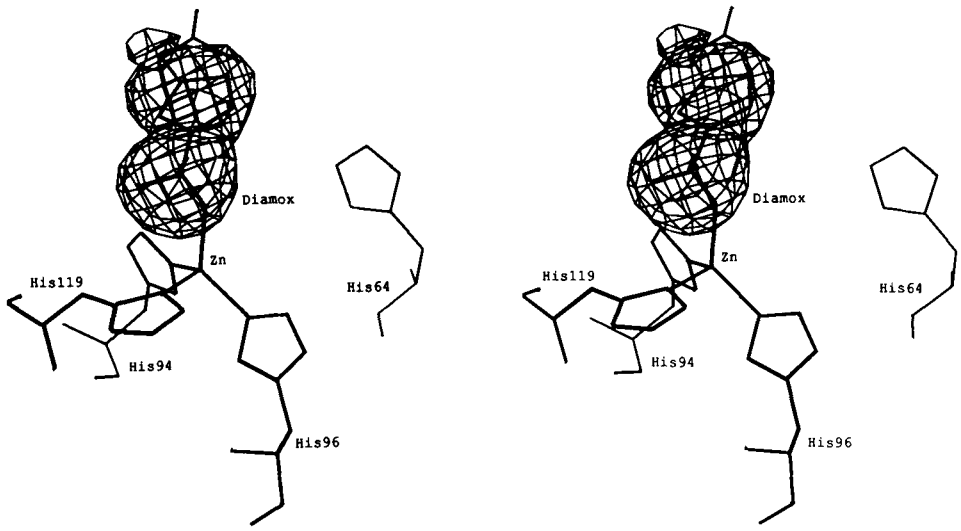

Fig. 5. Stereo drawing showing the $|F_{obs}(complex)| - |F_{calc}(native)|$ electron density map of the Diamox–HCA II complex at 3.0 Å resolution. Contours are drawn at $+3\sigma$.

indicating that all other histidine residues in the enzyme are unmodified. The occupancy of Hg^{2+} ions at His-64 relative to the occupancy at Cys-206 was determined to 0.58 and 0.49 for the Nδ1 and Nϵ2 bound Hg^{2+}, respectively.

AMS and Diamox

The difference electron density of the sulfonamide complex indicates no large changes in the protein structure. The rms deviation for the α-carbon atoms of the AMS structure superimposed on the native structure is 0.085 Å. Three mercury ions bind to the protein in the AMS-inhibited structure. One binds at the SH group of Cys-206, the second at the Nδ1 atom of His-64, and the third, the AMS mercury, at the Nϵ2 atom of His-64. This means that the three mercury-binding sites identified in the mercury-inhibited enzyme described above are also occupied in the AMS-inhibited structure. The free mercury ions have probably dissociated from AMS molecules in the crystallization solution. Cys-206 is the only residue in the AMS structure that deviates more than 1.0 Å when compared to the native enzyme. Its side chain can take two orientations: in the native enzyme it is oriented inward but when bound to mercury the γ-sulfur is pointing outward. The electron density of the AMS molecule is well defined over the sulfonamide group that binds to the zinc ion (see Fig. 3), most probably through the nitrogen atom of the sulfonamide group.[22,23] Spectroscopic data also suggest that sulfonamide inhibitors are bound as anions, $R\text{-}SO_2NH^-$.[23,24] The electron density over the benzene ring is not as well defined due to ripple effects from the AMS mercury ion. The AMS amide group is situated 2.0 Å from the zinc ion and has replaced the zinc-bound hydroxyl ion in the native structure with a shift in position of 0.4 Å. The geometry around the zinc ion is described in Table I. Just like the hydroxyl ion, the amide proton forms a hydrogen bond with the Oγ1 atom of Thr-199 that is 2.8 Å away. One of the oxygens of the sulfonamide group displaces the "deep water" of the native structure with a shift of 0.8 Å. This oxygen forms a hydrogen bond to the

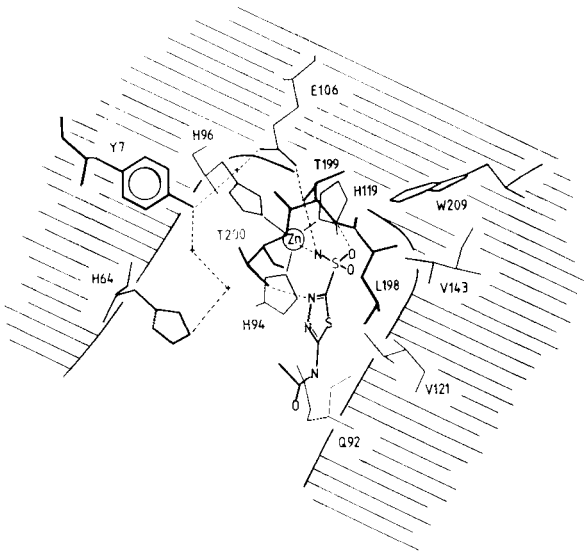

Fig. 6. Schematic drawing of the Diamox inhibitor binding to HCA II. The molecule makes van der Waals' contacts with Val-121, Val-143, Leu-198, and Gln-92 in the hydrophobic side of the active site cavity.

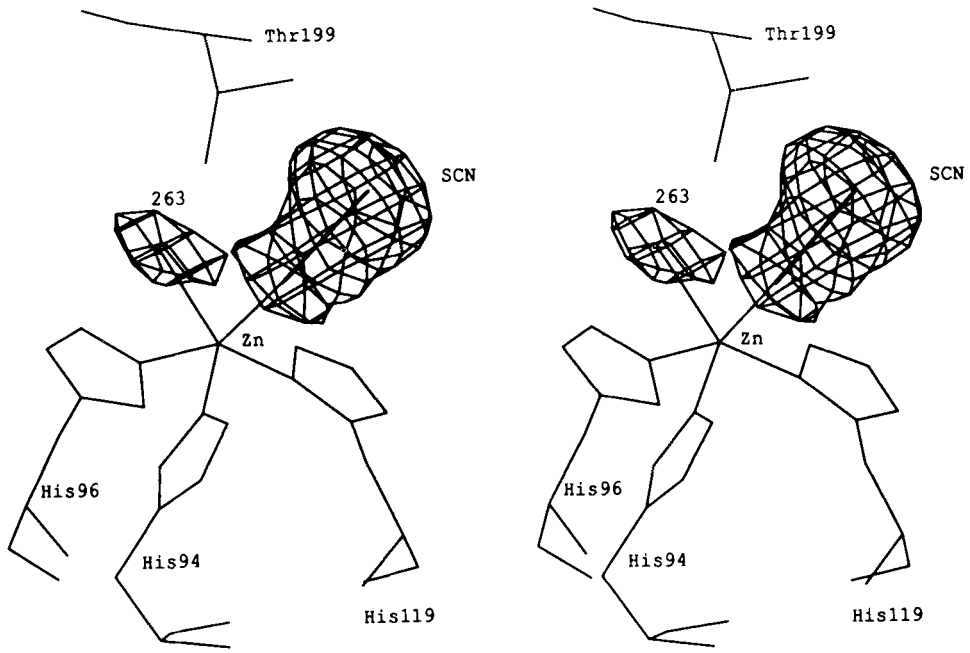

Fig. 7. Stereo drawing showing the $|F_{obs}| - |F_{calc}|$ electron density map over the SCN^-–HCA II complex at 1.9 Å resolution. Contours are drawn at $+3\sigma$. The SCN^- ion and the zinc-bound water molecule were not included in the structure factor calculations.

TABLE I. Geometry of the Zinc Ion in the AMS-Inhibited HCA II

	Distance to zinc (Å)	Angles (°) X–Zn-N (AMS)	X–Zn-94	X–Zn-96	X–Zn-119
O (AMS)	3.1	48	89	164	81
N (AMS)	2.0	—	111	117	107
Nε2 94	2.0	—	—	104	116
Nε2 96	2.1	—	—	—	101
Nδ1 119	1.8	—	—	—	—

TABLE II. Geometry of the Zinc Ion in the SCN^--Inhibited HCA II

	Distance to zinc (Å)	Angles (°) X–Zn-263	X–Zn-94	X–Zn-96	X–Zn-119
N (SCN^-)	1.9	70	91	155	95
Wat 263	2.2	—	100	89	146
Nε2 94	2.1	—	—	107	110
Nε2 96	2.1	—	—	—	95
Nδ1 119	1.9	—	—	—	—

TABLE III. Hydrogen Bonding Distances in the Active Site of SCN^--Inhibited HCA II

Bond	Distance (Å)
263 OHH–318 OHH	2.6
263 OHH–N SCN^-	2.4
263 OHH–Oγ1 Thr-199	2.7
264 OHH–292 OHH	2.9
264 OHH–Oη Tyr-7	2.9
265 OHH–Oη Tyr-7	2.7
265 OHH–Oε2 Glu-106	2.5
265 OHH–O Thr-199	3.0
292 OHH–318 OHH	2.7
292 OHH–369 OHH	2.4
318 OHH–389 OHH	3.2
318 OHH–Oγ1 Thr-200	3.1
332 OHH–Nδ1 His-64	2.6
369 OHH–Nδ2 Asn-62	3.3
369 OHH–Nδ2 Asn-67	2.5
385 OHH–Nε2 His-64	2.6
Oδ1 Asn-62–N His-64	3.0
Oε1 Gln-92–Nδ1 His-94	2.7
Nδ1 His-96–O Asn-244	2.7
Oε1 Glu-106–Oγ1 Thr-199	2.5
Oε2 Glu-106–N Ile-246	2.9
Oε2 Glu-117–Nε2 His-119	2.8

main chain N atom of Thr-199 (3.1 Å) and is 4.1 Å from the zinc ion. The second sulfonamide oxygen does not form any hydrogen bond to other residues but is within van der Waal's distances from Val-121 and Val-143 and is 3.1 Å away from the zinc ion. The location of the AMS molecule in the active site is shown schematically in Figure 4. The benzene ring is situated toward the hydrophobic part of the cavity and makes van der Waals' interactions with Gln-92, Val-121, Leu-198, and Thr-200. The amino group forms hydrogen bonds with one water molecule near the cavity entrance.

The electron density map for the Diamox-inhibited enzyme is not as well defined due to lower resolution (see Fig. 5). This makes it difficult to exactly assign the positions of the atoms in the sulfonamide group. However, the electron density is consistent with the same position and orientation of the sulfonamide group as for AMS, i.e., with only the nitrogen bound to the zinc ion. Like AMS the Diamox molecule extends toward the hydrophobic side of the cavity and the thiadiazole ring forms van der Waals' interactions with Gln-92, Val-121, and Leu-198. One nitrogen on the thiadiazole ring forms a hydrogen bond with the Oγ1 atom of Thr-200. The electron density over the acetylamido group is poorly defined, making it impossible to assign its location. The interactions between the Diamox molecule and different amino acids are illustrated in Figure 6.

SCN^-

The refined protein model of the SCN^-–HCA II complex is generally identical to the refined native model. The side chains of Lys-9, Ser-43, Lys-159, Asn-253, and Lys-257 show bad electron density. The rms deviation for the α-carbon atoms of the SCN^- structure superimposed on the native structure is 0.125 Å. Residues with rms deviations higher than 1.0 Å are Lys-9, Gln-136, Cys-206, Gln-255, and Lys-257. These residues, except Cys-206, are situated on the surface of the protein with their side chains protruding outward. The reorientation of Cys-206 is due to its partial labeling by PCMBS since in the native structure, the Cys-206 side chain points inward. The refined temperature factors for individual residues are in general higher than in the native structure, perhaps due to different techniques in data collection for the two structures.

In addition to the three histidyl residues electron density for two more ligands were observed associated with the zinc ion. This electron density was interpreted as originating from one SCN^- ion and one water molecule. Both ligands have high temperature factors (32 and 40 $Å^2$, respectively) after refinement, which probably reflects a low occupancy

consistent with the low affinity for SCN^- ion at high pH.[4–6] This can also be seen in the weak electron density over the nitrogen atom and the water molecule in $2|F_{obs}| - |F_{calc}|$ maps. The weak electron density might also be due to ripple effects from the zinc ion. However, the final $|F_{obs}| - |F_{calc}|$ map shows well-defined electron density both for all the inhibitor atoms and for the zinc-bound water molecule (see Fig. 7). One of the new ligands, the nitrogen atom of the SCN^- ion, is situated 1.9 Å from the zinc ion but shifted 1.3 Å from the position of the hydroxyl ion in the native enzyme and 1.1 Å from the position of the AMS sulfonamide nitrogen. Its distance to the Oγl atom of Thr-199 is 3.6 Å, a distance too large for a hydrogen bond. However, the strong hydrogen bond (2.4 Å) between the Oγl atom of Thr-199 and Oε1 of Glu-106 in the native structure is maintained (2.5 Å) in the inhibitor complex. The second ligand, the water molecule 263† is situated 2.2 Å from the zinc ion at a difference of 1.2 Å from the position of the hydroxyl ion in the native structure and 3.7 Å from the position of the AMS oxygen situated closest to the zinc. This water forms hydrogen bonds to the Oγl atom of Thr-199 (2.7 Å) and to water molecule number 318 (2.6 Å). The water-to-SCN^- distance is 2.4 Å. The resulting pentacoordinated geometry of the zinc ion is given in Table II. The SCN^- ion extends into the hydrophobic part of the cavity with the sulfur atom 1.2 Å from the position of the displaced "deep" water molecule. The sulfur atom is situated 4.1 Å from the main chain N atoim of Thr-199 and makes van der Waals' interactions with Val-143, Leu-198, and Trp-209 (see Fig. 8).

The hydrogen bond network in the active site is almost identical to the native structure. The largest shifts in position are 0.7 and 0.6 Å for water molecules 385 and 318, respectively. Most bond distances in the active site of the SCN-inhibited complex are given in Table III.

DISCUSSION

Several aspects of the catalytic mechanism of carbonic anhydrase remain unclear such as the site for the substrate binding and its relation to the zinc's geometry. The new results from this crystallographic study of three different types of HCA II inhibitors enable us to propose a probable substrate-binding site and provide new information for a proposed catalytic mechanism.

Mercuric ions have been suggested to inhibit the enzyme by binding to His-64,[10] which was believed to serve as a proton transfer group between the zinc-bound water molecule and the solvent buffer molecules.[25] However, the validity of this model is not established since replacement of His-64 with other residues (Lys, Ala, Glu, and Gln), by site-directed mutagenesis, causes only a small reduction in the CO_2 hydration activity.[26] These mutated residues cannot function as good proton transfer groups during catalysis. Our crystallographic investigations verify that mercuric ions can bind to either nitrogen of His-64. In view of the previous results the inhibitory effect of this binding is hard to interpret. Maybe it is due to the extra change introduced or simply because the water structure in the active site is distorted.

We have reinvestigated the binding of both AMS and Diamox in HCA II using phase angles from our highly refined model.[3] To improve the stereochemistry, some refinement of the AMS complex has been done. The nitrogen of the sulfonamide group replaces the zinc-bound hydroxyl ion and the closest sulfonamide oxygen is situated 3.1 Å from the zinc ion. This binding is in accordance with earlier descriptions,[2] but our interpretations of the results are somewhat different. Whereas they suggested[2] that the oxygen of the sulfonamide group is a fifth ligand to the zinc ion, we consider 3.1 Å to be too large a distance for anything but a weak interaction with the zinc, thus the tetrahedral geometry of the zinc ion is maintained. This is further supported by the visible[27] and X-ray[28] absorption spectra. Although the sulfonamide inhibitors are generally believed to bind to the zinc in a fashion similar to the transition state binding of HCO_3^-, for reasons that will be discussed we do not believe that this is the case since the proton and charge distribution on the sulfonamide ligands are not equal to the distibution on the substrate ligands.

Spectroscopic studies on HCA II indicate that the SCN^- ion binds to the zinc by increasing its coordination number. [7,8] Our present crystallographic investigations are in agreement with these results. We have identified one SCN^- ion and one water molecule as ligands to the zinc ion. The zinc-ligand angles in the SCN^--inhibited structure (see Table II) may best be described as a square pyramidal arrangement of ligands, i.e., octahedral-like with one vacant coordination site. This geometry is similar to the pentacoordinated zinc ion in the refined structures of carboxypeptidase A [29,30] and hydroxamic acid-inhibited thermolysin[31] (cf. Tables IV and II).

The relocation of the SCN^- nitrogen with respect to the hydroxyl group in the native structure is also due to its proximity to the Oγl atom of Thr-199. Hydrogen bond donor-acceptor relations in the active site suggest that this Oγl atom can serve as the hydrogen bond acceptor only from the hydroxyl ligand since its proton form a hydrogen bond with Glu-106.[3] The equivalent hydrogen bond cannot be made by SCN^-, and the inhibitor nitrogen is placed 0.9 Å further away than the hydroxyl ion, thus making a van der Waals' contact rather than a hydrogen bond. In the HCA II–SCN^- complex the Oγl atom of Thr-199 does not change position and maintains its dis-

†Note that the tetrahedrally coordinated hydroxyl con in the native HCA II model and the pentacoordinated water molecule in the SCN-HCA II are given the same number, 263.

TABLE IVa. Geometry of the Zinc Ion in Carboxypeptidase A[29,30]

	Distance to zinc (Å)	Angles (°)			
		X–Zn-Oε2 72	X–Zn-69	X–Zn-196	X–Zn-571
Oε1 Glu-72	2.2	56	91	156	96
Oε2 Glu-72	2.3	—	121	101	114
Nδ1 His-69	2.1	—	—	99	116
Nδ1 His-196	2.1	—	—	—	99
Wat 571	2.0	—	—	—	—

TABLE IVb. Geometry of the Zinc Ion in the L-Leucyl-Hydroxylamine (LLH)-Inhibited Thermolysin (as Measured From the Available Coordinates[31])*

	Distance to zinc (Å)	Angles (°)			
		X–Zn–OH LLH	X–Zn-142	X–Zn-146	X–Zn-166
O LLH	2.0	69	110	138	93
OH LLH	2.1	—	101	73	135
Nε2 His-142	2.3	—	—	94	124
Nε2 His-146	2.0	—	—	—	103
Oε1 Glu-166	2.0	—	—	—	—

*O and OH represent the hydroxamate carbonyl and hydroxyl oxygen, respectively.

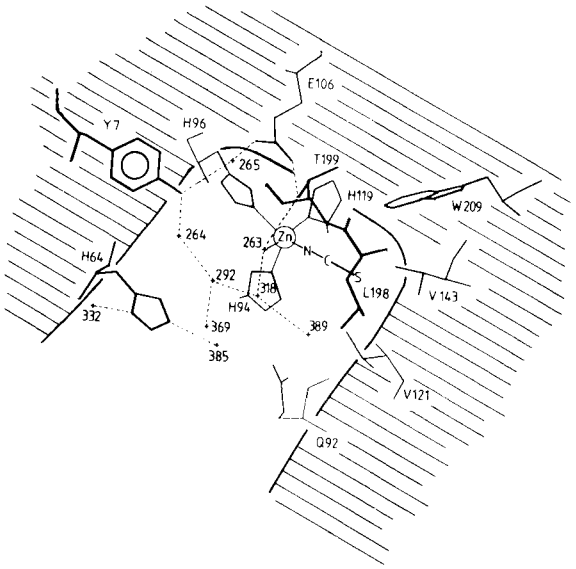

Fig. 8. Schematic drawing of the binding of SCN^- inhibitor in HCA II. The nitrogen atom is bound to the zinc ion whereas the rest of the molecule replaces the "deep" water 338 in the native enzyme. The sulfur atom makes a van der Waals' interaction with Val-143, Leu-198, and Trp-209.

ance to both Glu-106 and the zinc-binding water molecule. The water molecule also forms a hudrogen bond to water molecule 318 and probably also a hydrogen bond to the SCN^- nitrogen.

We have thus observed three separate binding sites on the zinc ion (now referred to as A, B, and C sites) for ligands from the solvent. These sites can be occupied by inhibitors, substrates, water molecules, or hydroxyl ions. In addition there are also two protein atoms that make important contacts with the ligands; the main chain N atom and the Oγl atom of Thr-199. The N atom of Thr-199 is always a hydrogen bond donor and interacts normally with a water molecule (the "deep" water), but can also bind to inhibitor molecules (e.g., one oxygen of AMS). The Oγl atom of Thr-199 can function only as a hydrogen bond acceptor since it has a strong hydrogen bond to Glu-106 that is changed despite its buried location in the structure.[3] This restriction on the Oγl atom is probably one of the most important features in the active site of carbonic anhydrases.[32] The site A on the zinc ion is between the B and C sites and given the zinc tetrahedral geometry when the three imidazole ligands are included. This site can primarily be occupied by protonated but negatively charged ions like OH^- or the $R–SO_2NH^-$ in sulfonamides. The proximity to the Oγl atom of Thr-199 does not easily permit nonprotonated ions to bind to this site. Such ions (like SCN^-) will instead bind to site B at van der Waals' distance from Oγl. This leaves a large area of the zinc exposed as well as leaving Thr-199 without a hydrogen bond donor, thus creating a natural binding site (site C) for a water molecule. It is possible to speculate about the binding of water molecules to the zinc ion at low pH. Since there seems to be no absolute requirement for a tetrahedral geometry, possibly two water molecules can bind to the zinc ion.

The three observed binding sites are obviously of central importance for the discussion of the catalytic mechanism of carbonic anhydrase. We have concluded through model building studies that a bicarbonate ion can be placed with its negative charge at site B and its protonated oxygen at site C. In Figure 9 we have outlined a catalytic mechanism in agreement with the mechanism proposed by Lindskog et al.[1] What has not been discussed before are the details of the stereochemistry of the substrate binding. The mechanism is to some extent also consistent with the mechanism made by Kannan et al.[32] in that it emphasizes the significance of the hydrogen bonds:

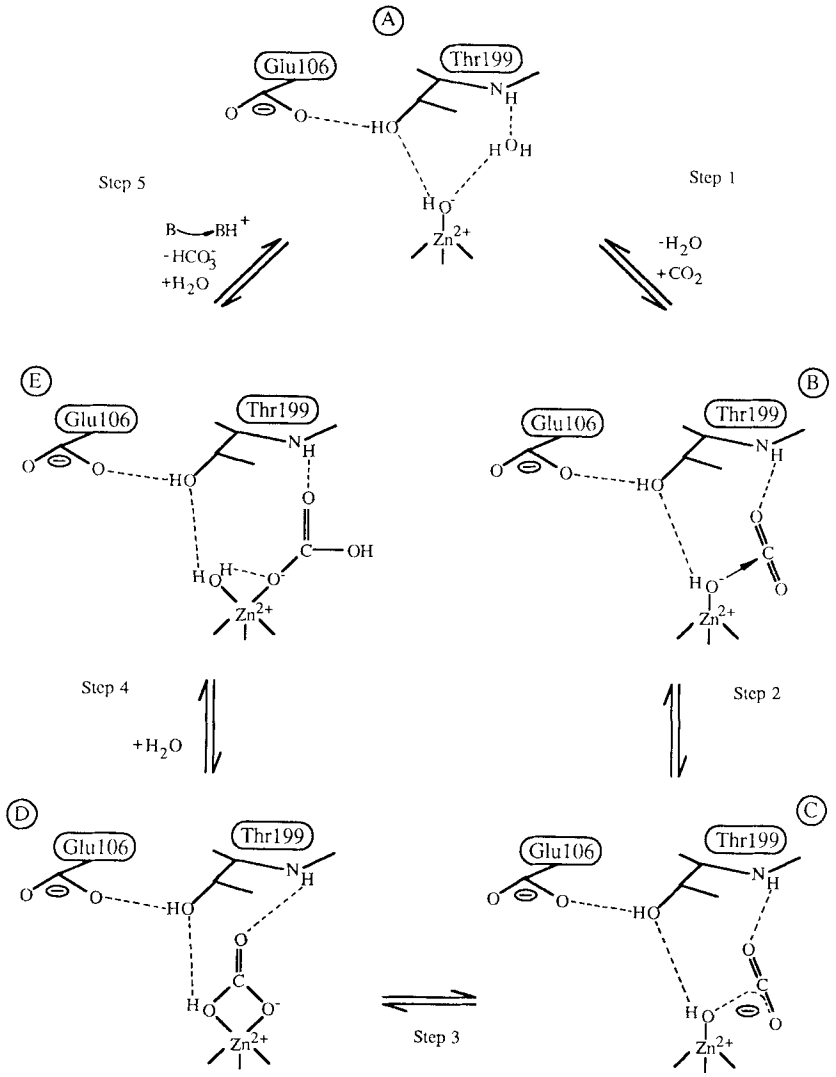

Fig. 9. Suggested catalytic mechanism of carbonic anhydrase. Step 1: Binding of CO_2 close to zinc. Nucleophilic attack of the OH^- group on the carbon atom. Step 2: Charge delocalization in HCO_3^-. Step 3: Conformational change at the zinc, i.e., both the protonated and charged oxygen form ligands to the zinc. Step 4: Breaking of the zinc–OH bond. The OH moiety is replaced on the zinc by a water molecule. A tentative hydrogen bond between the water molecule and the oxygen ligand is indicated. Step 5: Product release and ionization of the zinc-bound water molecule to a hydroxyl ion by proton transfer to a buffer molecule. Of the different stages presented A is consistent with the native structure of HCA II with an OH^- ion bound at "site A"; stage B with the position of the sulfonamide ligands in AMS with its NH^- moiety bound at "site A" and one of its oxygen at a position 3.1 Å from the zinc ion; stage E with the SCN^--inhibited structure with its N^- atom bound at "site B" and a water molecule bound at "site C."

solvent–Thr-199–Glu-106, even though a direct proton transfer to Glu-106 does not need to be considered. The mechanism illustrated in Figure 9 is described in five steps. Step 1: CO_2 binds near the zinc ion with one oxygen atom replacing the deep water and with the second oxygen atom possibly situated 3.1 Å from the zinc as in the AMS binding, i.e., in the hydrophobic pocket close to residues Val-121, Val-143, and Trp-209. This is in agreement with theoretical studies including quantum mechanical[33] and chemical dynamic[34] calculations that favor a bond distance of 2.9 and 2.6 Å, respectively, between the CO_2's oxygen and the zinc. The zinc-bound hydroxyl ion makes a nucleophilic attack on the carbon of CO_2 which, in step 2, delocalizes the negative charge from the hydroxyl ion to one of the CO_2 oxygens. Step 3: The negatively charged oxygen binds to the zinc at the "B site" simultaneously as the uncharged hydroxyl group moves to the position of the "C site" while still hydrogen bonding to the Oγl atom of Thr-199. This type of pentacoordinated binding of the substrate has been suggested from theoretical calculations,[33] and from the rates of CO_2–HCO_3^- interconversion estimated both from ^{13}C NMR resonance studies[35] and from ^{18}O exhange experiments.[36] Paramagnetic ^{13}C NMR relaxation measurements also indicate a bond distance

of 2.7 Å between the ^{13}C atom of HCO_3^- and Mn(II) at high pH.[37] Model building studies of HCO_3^- with one oxygen at the "B site" and a second at the "C site" show a distance of about 2.5 Å between the carbon of HCO_3^- and the zinc ion. Step 4: The bond between the zinc ion and the OH moiety of the bicarbonate breaks and a water molecule moves into its place. Step 5: The catalytic cycle is completed by product releases. Most kinetic data are consistent with a HCO_3^- release followed by a rate-limiting proton transfer from the zinc-bound water molecule to a buffer molecule (for a review see ref. 38). However, with a negatively charged oxygen ligated to the zinc ion the bicarbonate ion does not seem to be a good leaving group. Thus, it seems more likely that the proton transfer from the zinc-bound water molecule to the buffer molecules is what enables the release of the bicarbonate ion. More investigations may be needed before the product release part of the reaction can be elucidated.

An internal proton transfer within the bicarbonate molecule has been suggested by Liang and Lipscomb.[39] Their chemical dynamic calculations show that there is no high-energy barrier to prevent such a transfer and that it would indeed be greatly facilitated by suitably positioned water molecules. In fact water molecules number 318 and 389 both in the native structure and in the SCN^- complex seem to be appropriately placed for such a function. The existence of two binding sites on the zinc ion makes this type of transfer unneccessary but does not eliminate it. Alkyl carbonate esters have been reported to function not as substrates but as anionic inhibitors of CA.[5] Liang and Lipscomb[39] cited this lack of activity as support for their mechanism. However, from the crystallographic structure it is clear that an alkyl group at the position of the proton in HCO_3^- will prevent binding at the "C site." Presumably, alkyl carbonates bind with their negatively charged oxygen at the "B site."

The combination of site-directed mutagenesis, spectroscopic methods, and X-ray crystallography should improve the possibility of better identifying the regions for substrate binding. In particular, modifications that inhibit the elusive proton transport part of the reaction need to be studied.

ACKNOWLEDGMENTS

We are grateful for support and valuable discussions with Prof. Sven Lindskog, University of Umeå, Sweden. Dr. Jan Sedzik is thanked for help in processing part of the diffraction data of the SCN^--inhibited complex, Dr. Torsten Unge for advice and assistance during the purification of native HCA II enzyme, and Terese Bergfors for help with the manuscript. These studies have been supported by the Swedish Natural Science Research Council.

REFERENCES

1. Lindskog, S., Engberg, P., Forsman, C., Ibrahim, S.A., Jonsson, B.-H, Simonsson, I., Tibell, L. Kinetics and mechanism of carbonic anhydrase isoenzymes. Ann. N.Y. Acad. Sci. 429:61–75, 1984.
2. Kannan, K.K. Vaara, I., Notstrand, B., Lövgren, S., Borell, A., Fridborg, K., Petef, M. Structure and function of carbonic anhydrase: Comparative studies of sulphonamide binding to human erythrocyte carbonic anhydrases B and C. In: "Drug Action at the Molecular Level." Roberts, G.C.K. ed. New York: Macmillan, 1977: 73–93.
3. Eriksson, A.E., Jones, T.A., Liljas, A. The refined structure of human carbonic anhydrase II at 2.0 Å resolution. Proteins 4:274–282, 1988. (The preceding article.)
4. Pocker, Y., Deits, T.L. Effects of pH on the anionic inhibition of carbonic anhydrase activities. J. Am. Chem. Soc. 104:2424–2434, 1982.
5. Pocker, Y., Deits, T.L. The bicarbonate proton in carbonic anhydrase catalysis. J. Am. Chem. Soc. 105:980–986, 1983.
6. Tibell, L., Forsman, C., Simonsson, I., Lindskog, S. Anion inhibition of CO_2 hydration catalyzed by human carbonic anhydrase II. Biochim. Biophys. Acta 789:302–310, 1984.
7. Bertini, I., Canti, G., Luchinat, C., Scozzafava, A. Characterization of cobalt(II) bovine carbonic anhydrase and of its derivatives. J. Am. Chem. Soc. 100:4873–4877, 1978.
8. Bertini, I., Lanini, G., Luchinat, C., Raciti, A. Are there other acidic groups capable of affecting the electronic spectra of cobalt(II) substituted carbonic anhydrase? Inorg. Chim. Acta 91:173–177, 1984.
9. Magid, E. The activity of carbonic anhydrases B and C from human erythrocytes and the inhibition of the enzymes by copper. Scand. J. Haematol. 4:257–270, 1967.
10. Tu, C., Wynns, G.C., Silverman, D.N. Inhibition by cupric ions of ^{18}O exchange catalyzed by human carbonic anhydrase II. J. Biol. Chem. 256:9466–9470, 1981.
11. Tilander, B., Strandberg, B., Fridborg, K. Crystal structure studies on human erythrocyte carbonic anhydrase C. J. Mol. Biol. 12:740–760, 1965.
12. Eklund, H., Nordström, B., Zeppezauer, E., Söderlund, G., Ohlsson, I., Boiwe, T., Söderberg, B.-O., Tapia, O., Bränden, C.-I., Åkeson, Å. Three-dimensional structure of horse liver alcohol dehydrogenase at 2.4 Å resolution. J. Mol. Biol. 102:27–59, 1976.
13. Steigemann, W. Die Entwicklung und Anwendung von Rechenverfahren und Rechenprogrammen zur Strukturanalyse von Proteiner am Biespiel des Trypsininhibitor Komplexes, des freien Inhibitors und der L-Asparaginase. Ph.D. thesis, Technical University Munich, 1974.
14. Liljas, A., Kannan, K.K., Bergstén, P.-C., Waara, I., Fridborg, K., Strandberg, B., Carlbom, U., Järup, L., Lövgren, S., Petef, M. Crystal structure of human carbonic anhydrase C. Nature New Biol. 235:131–137, 1972.
15. Adams, M.J., Haas, D.J., Jeffery, B.A., McPherson, A., Jr., Mermall, H.L., Rossmann, M.G., Schevitz, R.W., Wonacott, A.J. Low resolution study of crystalline L-lactate dehydrogenase. J. Mol. Biol. 41:159–188, 1969.
16. Jones, T.A. A graphics model building and refinement system for macromolecules. J. Appl. Crystallogr. 11:268–272, 1978.
17. Jones, T.A. FRODO: A graphics fitting program for macromolecules. In: "Computational Crystallography." Sayre, D. ed. Oxford: Clarendon Press, 1982: 303–317.
18. Bergstén, P.-C., Waara, I., Lövgren, S., Liljas, A., Kannan, K.K., Bengtsson, U. Crystal structure of human erythrocyte carbonic anhydrase C.V. Complexes with some anion and sulphonamide inhibitors. In: "Oxygen Affinity of Hemoglobin and Red Cell Acid-Base Status. Rörth, M., Astrup, P. eds. Copenhagen: Munksgaard; New York: Academic Press, 1971: 363–383.
19. Hendrickson, W.A., Konnert, J.H. Incorporation of stereochemical information into crystallographic refinement. In: "Computing in Crystallography." Diamond, R., Ramaseshan, S., Venkatesan, K. eds. Bangalore: Indian Institute of Science, 1980: 13.01–13.23.
20. Rossmann, M.G. Processing oscillation diffraction data for very large unit cells with an automatic convolution technique and profile fitting. J. Appl. Crystallogr. 12:225–238, 1979.

21. Schmid, M.F., Weaver, L.H., Holmes, M.A., Grütter, M.G., Ohlendorf, D.H., Reynolds, R.A., Remington, S.J., Matthews, B.W. An oscillation data collection system for high-resolution protein crystallography. Acta Crystallogr. A37:701–710, 1981.
22. Eveloch, J.L., Bocian, D.F., Sudmeier, J.L. Evidence for direct metal-nitrogen binding in aromatic sulfonamide complexes of cadmium(II)-substituted carbonic anhydrases by cadmium-113 nuclear magnetic resonance. Biochemistry 20:4951–4954, 1981.
23. Kanamori, K., Roberts, J.D. Nitrogen-15 nuclear magnetic resonance study of benzenesulfonamide and cyanate binding to carbonic anhydrase. Biochemistry 22:2658–2664, 1983.
24. Chen, R.F., Kernohan, J.C. Combination of bovine carbonic anhydrase with a fluorescent sulfonamide. J. Biol. Chem. 242:5813–5823, 1967.
25. Steiner, H., Jonsson, B.-H., Lindskog, S. The catalytic mechanism of carbonic anhydrase. Eur. J. Biochem. 59:253–259, 1975.
26. Forsman, C., Behravan, G., Jonsson, B.-H., Liang, Z.-W., Lindskog, S., Ren, X., Sandström, J., Wallgren, K. Histidine 64 is not required for high CO_2 hydration activity of human carbonic anhydrase II. FEBS Lett. 229:360–362, 1988.
27. Bertini, I., Luchinat, C. Cobalt(II) as a probe of the structure and function of carbonic anhydrase. Acc. Chem. Res. 16:272–279, 1983.
28. Yachandra, V., Powers, L., Spiro, T.G. X-Ray absorption spectra and the coordination number of Zn and Co carbonic anhydrase as a function of pH and inhibitor binding. J. Am. Chem. Soc. 105:6596–6604, 1983.
29. Rees, D.C., Lewis, M., Lipscomb, W.N. Refined crystal structure of carboxypeptidase A at 1.54 Å resolution. J. Mol. Biol. 168:367–387, 1983.
30. Rees, D.C., Howard, J.B., Chakrabarti, P., Yeates, T., Hsu, B.T., Hardman, K.D., Lipscomb, W.N. Crystal structures of metallosubstituted carboxypeptidase A. In: "Zinc Enzymes." Bertini, I., Luchinat, C., Maret, W., Zeppezauer, M. eds. Boston, Basel, Stuttgart: Birkhäuser, 1986: 155–166.
31. Holmes, M.A., Matthews, B.W. Binding of hydroxamic acid inhibitors to crystalline thermolysin suggests a pentacoordinate zinc intermediate in catalysis. Biochemistry 20:6912–6920, 1981.
32. Kannan, K.K., Petef, M., Fridborg, K., Cid-Dresdner, H., Lövgren, S. Structure and function of carbonic anhydrases. Imidazole binding to human carbonic anhydrase B and the mechanism of action of carbonic anhydrases. FEBS Lett. 73:115–119, 1977.
33. Pullman, A. Carbonic anhydrase: Theoretical studies of different hypotheses. Ann. N.Y. Acad. Sci. 367:340–355, 1981.
34. Liang, J.-Y. Carbonic anhydrase catalyzed CO_2 hydration: A theoretical study. Ph.D. thesis, Chapter III, Harvard University, 1987.
35. Simonsson, I., Jonsson, B.-H, Lindskog, S. A. ^{13}C nuclear-magnetic-resonance study of CO_2-HCO_3^- exchange catalyzed by human carbonic anhydrase C at chemical equilibrium. Eur. J. Biochem. 93:409–417, 1979.
36. Silverman, D.N., Tu, C.K., Lindskog, S., Wynns, G.C. Rate of exchange of water from the active site of human carbonic anhydrase C. J. Am. Chem. Soc. 101:6734–6740, 1979.
37. Led, J.J., Neesgaard, E. Paramagnetic carbon-13 NMR relaxation studies on the kinetics and mechanism of the HCO_3^-/CO_2 exchange catalyzed by manganese(II) human carbonic anhydrase I. Biochemistry 26:183–192, 1987.
38. Silverman, D.N., Lindskog, S. The catalytic mechanism of carbonic anhydrase: Implications of a rate-limiting protolysis of water. Acc. Chem. Res. 21:30–36, 1988.
39. Liang, J.-Y., Lipscomb, W.N. Hydration of carbon dioxide by carbonic anhydrase: Internal proton transfer of Zn^{2+}-bound HCO_3^-. Biochemistry 26:5293–5301, 1987.